A Revised Geometry for the Magnetic Wind of θ^1 Orionis C

Myron A. Smith

Catholic University of America,

3700 San Martin Dr., Baltimore, MD 21218;

msmith@stsci.edu

and

Alex W. Fullerton[1]

Dept. of Physics & Astronomy, University of Victoria,

P.O. Box 3055, Victoria, BC, V8W 3P6, Canada.

Version of February 2, 2008

---

[1]Postal Address: Dept. of Physics & Astronomy, The Johns Hopkins University, 3400 N. Charles St., Baltimore, MD 21218; awf@pha.jhu.edu

ABSTRACT

The star θ^1 Orionis C (O6–7 V) is often cited as a hot analog of Bp variables because its optical and UV line and X-ray continuum fluxes modulate over the magnetic/rotational period. In this circumstance, one expects emission and absorption components of the UV resonance lines to vary as a flattened magnetosphere co-rotates with the star. In this paper we re-examine the detailed velocity behavior of several strong UV lines. Whereas past work has focused on variations of the full profiles, we find that the blue and red wings of the C IV and N V resonance lines exhibit anticorrelated modulations. These appear as absorption excesses at large blueshifts, and flux elevations at moderate redshifts at the edge-on phase ϕ=0.5. No rest-frame absorption features, which are the typical signatures of cool, static disks surrounding Bp stars, can be detected at any phase.

We suggest that this behavior is caused by two geometrically distinct components of the wind, which are defined by the relationship between the extent of a magnetic loop and the local Alfven radius. Streams on field lines opening outside this radius are first channeled toward the magnetic equator, but after reaching the Alfven radius they are forced outward by radiative forces, eventually to become an expanding radial outflow. This wind component causes blueshifted absorption as the co-rotating magnetic equatorial plane crosses the observer's line of sight (ϕ= 0.5). The geometry of the inner component requires a more complicated interpretation. Wind streams first follow closed loops and collide at the magnetic equator with counterpart streams from the opposite pole. There they coalesce and fall back to the star along their original field lines. The high temperatures in these falling condensations cause the redshifted emission. The rapid circulation of these flows is likely the reason for the absence of signatures

of a cool disk (e.g., zero-velocity absorptions at $\phi \sim 0.5$) in the strong UV lines.

Subject headings: stars: individual (θ^1 Ori C) – stars: activity – stars: circumstellar matter – line: stars – magnetic fields

1. Introduction

The discovery by Donati et al. (2002) of a magnetic field in the periodic variable θ^1 Orionis C (HD 37022; O6–7 V: Morgan & Keenan 1973; O7: Stahl et al. 1996) solidified the expectation that it is a hot analog of the magnetic B-type variables, the so called He-anomalous Bp stars. In contrast to the Bp stars, the modulation of soft X-ray flux in θ^1 Ori C reveals the presence of a hot, co-rotating magnetosphere (Gagné et al. 1997). The magnetic and X-ray periods are presumed to correspond to the rotational period of 15.422 days, as determined from ultraviolet and optical line variations (Stahl et al. 1993, Stahl et al. 1996, Reiners et al. 2000). Nonetheless, questions have lingered as to how to reconcile the phased variations of strong optical and UV lines with the geometry of the Bp magnetosphere model (Donati et al. 2002).

The magnetic Bp variables can be classified as a subgroup of a larger class of early-type stars that includes at least two pulsating β Cephei stars (Henrichs et al. 1998), the "sn" stars[1] recently examined by Shore et al. (2004), and other related objects (e.g., Smith & Groote 2001; hereafter SG01). According to the usual picture, winds in magnetic Bp stars are prevented from escaping from the magnetic poles, but are channeled outwards along dipolar field loops. The wind is constrained to flow along these loops until it encounters streams from the opposite pole. When the two streams collide, they shock, cool, and either circulate back to the star or leak out through the outer disk edge where they are lost to the system. The initial formulation of this picture by Shore and collaborators (e.g., Shore & Brown 1990; hereafter SB90) envisaged polar outflows ("jets") and a cool, toroidal disk.

---

[1]The sn stars are a subgroup of the He-weak Bp stars. They are so named because of the broad or "nebulous" appearance of the helium lines in their spectra as well as the sharp, central components in the hydrogen and C II λ4267 lines.

Subsequent magnetostatic modeling of the wind flows of Bp stars by Babel & Montmerle (1997) has dealt with the post-shock cooling of the gas in the magnetospheric disk as the principal site of the UV and Hα line variations. In this formulation, rotation is so small as to be negligible. The frozen-in magnetosphere then resembles a wobbly inner tube that co-rotates with the Bp star. If the disk is extended enough in radius, it can contribute substantial line emission when it is viewed face-on. Moreover, disk regions passing in front of the star generally have a lower temperature than the photosphere and therefore remove additional flux from photospheric absorption lines. In the case of resonance lines, scattering of line flux has the same effect. Thus, over the cycle various viewing aspects of the wind/disk complex can produce a variety of emissions and absorptions in the UV resonance lines of Si IV, C IV, and N V. In addition, modulations of Hα emission (Short & Bolton 1994) and high-level Balmer line absorptions (Groote & Hunger 1976) provide excellent diagnostics for well-developed magnetospheres, such as the one surrounding the prototypical He-strong star σ Orionis E. Along the hot edge of the classical Bp domain, dense winds insure that the wind particles do not fractionate chemically, with the result that the surface abundances of these stars remain normal.

The study of the wind geometry of θ^1 Ori C is compelling because it is the only O star currently known to possess a magnetic field (Henrichs 2005). The presence of a strong field in a dense, high-velocity wind make its circumstellar environment a unique laboratory to study high-energy magnetohydrodynamic plasma (Babel & Montmerle 1997). The interaction of various components of the wind produces the excitation of hot gas visible in X-ray spectra (Gagné et al. 2005) and potentially in the far-UV. Also, despite the inhibition caused by the strong magnetic field, the mass-loss rate of θ^1 Ori C is several hundred times larger than then mass-loss rates typical of hot Bp stars (Donati et al. 2002). The strong stellar wind, together with the star's slow rotation rate, permit spectral features to be Doppler shifted outside the photospheric line profile, which provides an opportunity to map

the geometry of the wind over a wide range of stellar distances and azimuths.

2. A Sketch of a New Magnetic Geometry

In this study we adopt the values for the rotational and magnetic tilt angles i and β from the analysis of the longitudinal magnetic field curves by Donati et al. (2002): both parameters are close to 45°. These values are the same as those adopted by Stahl et al. (1996; hereafter S96) and nearly the same to those of Reiners et al. (2000; hereafter R00). However, as noted by Donati et al. (2002), the mapping between line variations and magnetic phase adopted by S96 implies that the magnetic pole is viewed face-on at $\phi = 0.5$, which is difficult to reconcile with the observed Hα absorption at this phase. Instead, the magnetic-field measurements of Donati et al. (2002) show conclusively that phase $\phi = 0.0$ corresponds to the passage of the north magnetic pole across the projected center of the star. At this phase, material in the equatorial plane is seen "face-on" by a distant observer. At $\phi = 0.5$, the north magnetic pole has rotated to a point on the star's "upper" limb and the south magnetic pole makes its only brief appearance at the star's "lower" limb. At this time the observer sees the post-shock magnetosphere (i.e., the material near the magnetic equator) edge-on. If the Bp paradigm of SB90 and SG01 were applicable, maximum Hα emission and excess absorption in UV resonance lines should be observed at $\phi = 0$ and 0.5, respectively. As we will see below, this is not the case. Furthermore, Donati et al. (2002) were unable to explain the 50 km s^{-1} blueshift in the centroid of the Hα emission component in the context of the Bp picture.

The configuration described in this paper, shown as a sketch in Figure 1, is much different from this standard Bp paradigm. Our geometry attributes the blueshifted absorption in the C IV resonance lines at $\phi = 0.5$ to a radially outflowing, high-velocity wind. The point marked "X" designates schematically the Alfven radius at the magnetic

equator. For a very slowly rotating star this is where a bifurcation occurs in wind stream trajectories (e.g., ud-Doula & Owocki 2002). All streams sketched in Fig. 1 are diverted toward the magnetic equator because the particles are constrained at first to flow along field lines by the dominant magnetic forces. However, wind streams originating from high magnetic latitudes follow less confined loops that eventually extend beyond the Alfven radius. As these loops traverse the Alfven radius, radiation pressure (which falls off less quickly with distance from the star) overwhelms the magnetic forces and drags the field radially outward. Thus, these streams evolve to become a concentrated outflow confined to low magnetic latitudes. In contrast, streams in the inner wind zone that originate from intermediate magnetic latitudes on the star remain confined and contribute or remove line flux only when they collide with one another, shock, and return to the star (§ 3.5). The fate of this wind component contrasts strongly with the formation of the quasi-static, corotating disk typical of Bp stars, and is the subject of much of the rest of this paper.

3. The Morphology of Spectral Features

3.1. Line profile morphology according to previous studies

In their seminal paper, S96 demonstrated that the emissions in Hα, He II λ4686, and the absorptions of the C IV and Si IV resonance doublets of θ^1 Ori C are regularly modulated over a period of 15.422 days. This value is assumed to be the stellar rotational period. Phases in magnetic Bp variables are traditionally reckoned from the time of magnetic maximum, i.e., from the transit of a magnetic pole across the observer's line-of-sight. Typically for these stars, if magnetic ephemerides are not available, the zero point is taken as the epoch of Hα emission maximum (equivalent width minimum). Because the central axis of the magnetosphere coincides with the magnetic plane, these zero points coincide.

Using this zero point and period, S96 and R00 measured the equivalent-width variations with phase for several strong UV resonance and optical excited lines. The variations exhibit a maximum at $\phi = 0$, and both groups of authors interpreted this as excess absorptions in the line cores. The variations in the UV resonance, Hα, Hβ (G. Wade, private communication), and He II λ4686 lines are also highly nonsinusoidal. As measured across the entire profile, the phased equivalent width variations have an "M"-shape centered at $\phi = 0.5$. The second maximum of the "M" is centered at $\phi \approx 0.6$–0.7 and is generally stronger than the first prong at $\phi = 0.4$. In the case of the Hα line, the local minimum at $\phi = 0.5$ arises at least partly from the brief appearance of a red emission component (Stahl et al. 1993).

3.2. A detailed look at the C IV and N V resonance lines

To reinvestigate the variations exhibited by the UV lines, particularly the C IV and N V resonance doublets, we retrieved the 22 high-dispersion *IUE* spectra of θ^1 Ori C obtained through the large aperture with the SWP camera from the Multi-Mission Archive at Space Telescope[2]. The basic features of the variations are shown in Figure 2, which llustrates the fluctuations in C IV as a function phase in in the form of a grayscale ("dynamic") spectrum. The format of Fig. 2 is similar to Figure 10 of S96, except that the mean profile has been subtracted from individual spectra in the time series rather than the profile near $\phi = 0$, and the difference spectra illustrated in the image have been smoothed over 1 Å intervals.

Fig. 2 shows that the variations in the C IV resonance doublet are dominated by enhanced absorption (darker shades) in the high-velocity region of the unusually shallow

P Cygni absorption trough. However, weaker variations are also present throughout the absorption trough and even extend into the redshifted part of the profile. The red-wing variations of the λ1548 line are confused by blending between the doublet components, but the corresponding variations of the λ1550 can be seen clearly in window "e" in the figure. As discussed below, the weaker variations exhibit different behavior as a function of phase than the high-velocity absorption excess.

3.2.1. Maximum and minimum absorption profiles

The C IV equivalent width-phase curves (e.g., Figure 8 in S96) show some interesting features, and we have already mentioned the "M-shaped morphology. These features, particularly those pertaining to the different dependences of fluxes across the line profile, can be investigated further by comparing the individual spectra at strategic phases. A prime example of this is the different manner in which the fluxes across the line profiles contribute to the equivalent width of the full profile. Since the maximum swing in equivalent widths occurs over the comparatively narrow phase range between 0.6 and 0.9, it is illuminating to compare the three available spectra at these phases. These spectra are shown in Figure 3. The large flux variations at wavelengths shorter than 1543 Å are the most obvious differences. However, we also note that the fluxes in the blue and red regions of the doublet vary in opposite senses. Notice that while profiles at $\phi = 0.5 - 0.6$ exhibit increased blue absorption relative to the profiles observed near $\phi = 0.0$, the red-wing flux of the C IV λ1550 line (the region labeled "e") is high relative to the wing in the observation at $\phi = 0.94$. Put another way, the flux of the red wing of λ1550 is high when the fluxes of the (blended) blue wing of the doublet is low, and vice versa, over the rotational cycle. The blue wing variations overwhelms the anticorrelated red-wing ones for the C IV lines, which is why a depiction of the variation of the equivalent width extracted from the full profile

conceals the red wing variation.

Figure 4 likewise shows observations of the N V $\lambda\lambda1238$, 1242 at the same phases as the previous figure. The blue-wing flux variations are again present, but in this case they are much smaller than for the C IV doublet. In fact, it is difficult to see a variation at all between phases 0.6 and 0.9. However, the red-wing variation, (unblended in the two N V components), as indicated also by the smoothed difference spectrum at the bottom of the figure, is clearly visible.

Another interesting feature of Figures 3 and 4 is that when allowance is made for the different local continuum levels, the amplitude of the red-wing variations is virtually the same for both components of the C IV and N V doublets. Although there are additional complications due to blending, the implication is that the variable component is formed in an optically thick medium.

3.2.2. Variation of the lines over the rotation cycle

The phase-resolved fluctuations in different regions of the C IV resonance doublet just discussed can be compared by plotting pseudo-equivalent widths extracted from different wavelength intervals. To provide quantitative measures of the line absorptions, we computed "equivalent width indices," which are summed "net" fluxes in a defined series of windows that span the line. We used the net fluxes to avoid the errors introduced by the ripple correction for high-dispersion *IUE* data processed with "NEWSIPS." The equivalent width index in a given window was computed as the ratio of the total flux in it to the total flux in the particular order of the echelle spectrum. Like genuine equivalent widths, larger, positive values of these indices indicate greater absorption. They can be measured with precision since they are independent of continuum placement errors, but they cannot be converted

to true equivalent widths in Angstroms. Error bars were determined from the median point-to-point fluctuations in the values of the indices. This criterion likely overestimates the uncertainties because of the slow variations of the index through the cycle.

When summed over the entire profile, our plots of the C IV indices mimic the equivalent-width curves presented by S96. However, the behavior in individual wavelength bins distributed across the weak P Cygni profile is markedly different. For example, the shortest wavelengths are dominated by a single, large-amplitude variation with maximum absorption near $\phi = 0.5$. In contrast, the indices formed from bins that sample the core and red wing reflect systematic, small variations in the red wing, as suggested by Fig. 3. These red-wing variations are illustrated in Figure 5 for C IV and N V. From this figure it is apparent that a sinusoidal variation (shown as a dashed line for reference) is not a good fit to the data. Fig. 5 also shows that the red-wing variations of the N V $\lambda 1242$ profile $(0 - +250 \ \mathrm{km \, s^{-1}})$ track the red-wing variations of the C IV doublet.[3]

We also find that a simple blue/red-profile dichotomy is an inadequate description of the variations of different regions of the C IV doublet with phase. In Figure 6 we represent fluxes in four additional 1-Angstrom bins at increasingly blueshifted portions of the absorption trough. At the bottom of the figure we replot the curve from the red-wing extraction of 1550 Å in shown in Fig. 5. The "M"-pattern is present in curves b and c, but in curve a, representing the most negative velocities, the two prongs have merged together. The same behavior is evident in the dynamic spectrum (Fig. 2).

---

[3]Analogous red-wing variations are not present in the Si IV resonance doublet, which is primarily a photospheric feature for O7 dwarfs.

3.2.3. The high- and intermediate-velocity outflows

According to the revised geometry of the wind flow, spectroscopic observers in the right-hand section of Fig. 1 will see the effects on the C IV line profiles of a collimated, high-velocity wind rotating into their line of sight as phase $\phi = 0.5$ approaches. Thus, the equivalent width indices extracted from the far-blue wing exhibit maximum absorption strength at this phase. The "M"-shaped curves for the near-blue wing and smaller velocities can also be explained by this same flow geometry. Between phases $\phi = 0.3$–0.4 and 0.6–0.7, the absorptions occur at positions in the line that correspond approximately to the wind terminal velocity multiplied by the cosine of the angle between the line-of-sight to the center of the star and the bisector line in the equatorial plane. Since the column responsible for the high velocity absorption at $\phi = 0.5$ is shifted to intermediate velocities just before and after this phase, a distant observer sees the maximum absorption at these times. The wind flows seen against the rest of the stellar disk at these times are changing their direction and are also accelerating rapidly. Consequently, the absorptions these flows impose on the line profile are distributed over a broader velocity range and thus have a smaller influence on the equivalent widths extracted from any one narrow wavelength window in the absorption trough.

3.3. Phase behavior of excited lines

3.3.1. The wind lines

In Table 1 we summarize the relevant properties of a selection of optical and UV lines of θ^1 Ori C reported in the recent literature. All of these lines show a phase modulation. We include the phases at which absorption equivalent widths of various lines attain their maximum absorption values. Those lines for which the "M"-morphology is most prominent

are denoted by phases "$0.4 - 0.6$." We also show two entries for the C IV $\lambda\lambda1548,1550$ doublet. Following S96, the first of these refers to the equivalent width across the full profiles, while the second describes the results for the red half of the profile only. A clear division can be made between the lines predominantly formed in the wind (i.e., the UV resonance lines, Hα, the emission in Hβ, and He II $\lambda4686$) and the lines largely formed in the stellar photosphere (e.g., the excited transitions of C IV and O III).

As already noted, Hα and He II $\lambda4686$ exhibit complicated emissions. At $\phi = 0.0$, a strong emission appears in the blue wing, and subtle variations interpreted by Stahl et al. (1993) as emission appear at $\phi = 0.5$ to the red of line center. According to the sketch in Figure 1, blueshifted emissions might be observed as the magnetic pole crosses the projected center of the star at $\phi = 0$; this possibility is addressed below. For now we note that the appearance of strong Hα emission (slightly blueshifted or otherwise, and discounting a nebular contribution) is unusual in the spectra of mid-O dwarfs. Its presence in spectra of θ^1 Ori C is certainly attributable to the unusual conditions in the magnetically-channeled wind.

3.3.2. Other excited lines: optical

S96 and R00 illustrated the modulations of several excited lines of He I, He II, C IV, and O III. Depending on the data quality, the absorption curves of these lines exhibit either a broad plateau centered at $\phi = 0.5$, or a shallow local "M"-minimum at this phase. Although these authors constructed these curves by measuring the whole profile, differentiation with velocity can be found in the dynamic spectra of O III $\lambda5592$ and C IV $\lambda5812$ presented in these papers. These depictions show the blue-to-red migration of an apparent absorption, with line center crossing at $\phi \approx 0.75$. The traditional interpretations for the origins of migrating subfeatures in line profiles of hot stars include surface spots due to chemical

inhomogeneities, photospheric velocity fields due to nonradial pulsations, or circumstellar clouds forced into co-rotation. The first of these alternatives is improbable in an O star having a chemically homogeneous wind. The second is problematical for several reasons, but in particular because the migrating features are present during only half the cycle. We will return presently to the third alternative, "co-rotating clouds," in the modified form of dense, infalling material.

3.3.3. Other excited lines: O V λ1371 and N IV λ1718

S96 noted that the strength of the excited O V λ1371 line exhibits phase-dependent variations, but they did not discuss its behavior in detail. Figure 7 shows the equivalent width indices from fluxes binned over the ranges from -300 to -100 $\mathrm{km\,s^{-1}}$ and from -100 to $+100$ $\mathrm{km\,s^{-1}}$ in the line profile. These curves demonstrate that "blue" and "central-red" indices follow the morphology of the variations in the C IV resonance lines (Fig. 5); i.e., the two halves of the line profiles show anticorrelated behavior. Thus, the blue half exhibits excess absorption at $\phi = 0.5$, probably because of the importance of the accelerating wind seen at this orientation. In contrast, the red half shows either less absorption or more emission at this phase.

We have repeated these extractions for the excited N IV λ1718 line. Although the curves are noisier, they show the same anticorrelated blue/red behavior.

3.4. Interpreting the red variations

We now return to the more complicated issue of the origin of the red-wing variations, e.g., in the C IV and N V resonance lines. Within the limits imposed by the data quality, these and other optical lines listed in Table 1 show the same variations in the phase range

0.3–0.7. This fact suggests that the fluctuations are formed in the same geometrical structures in the wind. Because the behavior of this ensemble of lines is similar regardless of their excitation and ionization potentials, we expect that they are formed in a region of thermal equilibrium that is denser than an O-star wind. The variations are probably optically thick, though further modeling is required to demonstrate this explicitly.

There are two basic interpretations for the red-wing variations: either they represent *excess absorption* at $\phi \approx 0.9-0.0$ or they represent *additional emission* at $\phi \approx 0.5-0.6$. The distribution of the circumstellar material is implicit in these interpretations. In particular, if the red-wind variations are interpreted as excess emission, the material must be centered (or nearly centered) on either the star's magnetic pole or its magnetic equator in order to produce equivalent-width curves that are symmetric about the pole-on and equator-on phases. We have identified three scenarios to address this issue:

Option i: Central and red-wing *absorption* observed at $\phi = 0.0$ in closed loops projected against the limb of the star. The absorbing wind streams have a net positive velocity component relative to the observer.

Option ii: Central and red-wing *emission* seen in the plane of the sky due to columns of material emanating from the magnetic poles. At $\phi = 0.5$ these columns have rotated to opposite limbs of the star.

Option iii: Central and red-wing *emission* from infalling material viewed edge-on in the magnetic equatorial plane.

Option i suggests that the variations are due to absorption that is redshifted with respect to an observer situated above the magnetic pole in Fig. 1. Thus, the gas responsible for it must be moving with a vector component directed away from the observer, even though the wind is predominantly flowing outward along the magnetic field lines in this

region. This configuration is difficult to achieve, though it might arise from wind streams moving along closed loops near the star. In this case, the line absorption would be visible at phases when the flow appears to cross the edge of the stellar disk. To explore this idea, we can estimate the fraction of the stellar disk occulted by such a wind stream in the most ideal circumstances. We have computed plasma absorptions using the Hubeny atmosphere and spectral synthesis and "cloud" transfer codes *SYNSPEC* and *CIRCUS* (see SG01 and Smith 2001) for a wind having a temperature of $35,000 - 40,000$ K. We find that in the "best" possible case for *Option i,* (i.e., for an optically thick wind with no background stellar-limb darkening), an absorption component formed at -200 km s^{-1} would have to be produced by streams covering at least 9% of the stellar disk with a column density in H of at least 10^{20} cm^{-2} in order to produce the redshifted variations observed in C IV and N V.

Even so, it is difficult to cover this much of the stellar disk with material that is redshifted by as much as $+400$ km s^{-1}; see Fig. 3. Since the wind streams near the stellar limb are moving nearly parallel to the stellar surface, speeds of ~ 1500 km s^{-1} are required to account for a projected component of 400 km s^{-1}. However, the terminal velocity of the wind in this star is no more than 2000 km s^{-1} (Walborn & Nichols 1994): for a line-driven stellar wind characterized by a $\beta=1$ velocity law, a velocity as large as 1500 km s^{-1} would only be reached at distances of $\sim 4 R_\star$; i.e., far from the stellar surface. In view of the implausible degree of fine-tuning required by *Option i*, we do not think it is likely.

Option ii has the advantage that Doppler-shifted emission is known to be present in some H and He lines at other phases, particularly $\phi = 0$, where it extends ~ 300 km s^{-1} redward of line center (Stahl et al. 1993; S96; G. Wade, private communication). Since the behavior of the UV resonance lines is similar, it is reasonable to conclude that their variations are also due to changes in emission.

According to *Option ii,* scattering brings flux into our line of sight when the north

magnetic pole rotates to the stellar limb. An observer to the right in Fig. 1 observes a glowing column of particles moving through the plane of the sky. However, as the column ("jet") fans out from the plane of the sky, we expect to see primarily blueshifted Hα emission unless the line is optically thin. Thus, this picture fails to explain the exclusively redshifted emission observed in C IV and N V. Perhaps the idea could be saved by invoking a significant departure from magnetic axi-symmetry, e.g., with a decentered dipole and a jet that is compressed in one 180° azimuthal sector. In such a scheme the observer might see more gas receding over a large area of the sky than gas exhibiting blueshifts in the foreground. However, even this geometry would produce significant blueshifted emission, which is not indicated in Figs. 2, 3 or 4. Thus, *Option ii* is probably not viable.

Option iii associates the emission maximum at $\phi = 0.5$ with infalling material near the magnetic equator rather than the poles. Since the lines of sight to this emission are also those that intersect the high-velocity wind moving toward the observer at this phase, this idea seems at first counterintuitive. How can the wind along the central line of sight to the star be approaching and receding at the same time? Furthermore, this scenario must explain the appearance of redshifted in many strong lines, including Hα (Stahl et al. 1993). In the resonance lines, the emission is probably optically thick. Moreover, since both low- and high-excitation lines show emission, it is most likely formed in a dense circumstellar medium and thus probably close to the star. The geometry illustrated in Fig. 1 addresses these issues, in particular by showing how rapidly moving, red- and blue-shifted material can be found between between the star and a distant observer at $\phi = 0.5$.

3.5. The infalling wind picture

The presence of the infalling material required by *Option iii* is is largely confirmed by recent magnetohydrodynamic (MHD) simulations by Dr. A. ud-Doula (private

communication; see Gagné et al. 2005 for a description of this work), which also provide a physical basis for the geometry sketched in Fig. 1. As with previous studies of Bp stars, the circulation results from the collision of wind streams that originate in opposite magnetic hemispheres and are guided by closed loops toward the magnetic equator. In the case of θ^1 Ori C, which has a much denser wind than a typical Bp star, the collisions at the magnetic equator result in the formation of dense, optically thick blobs. These structures cannot be supported by radiation pressure from the star, and fall back toward the surface. Since the blobs are still constrained to move along magnetic fields lines, they fall obliquely back toward the star along the lines that originally carried them to the magnetic equator. Observers viewing the system edge-on ($\phi = 0.5$) will see the infall as a redshifted, optically thick feature; in spectra with sufficiently high signal-to-noise ratio, this emission might be variable from one cycle to the next. Ud-Doula's models also include effects of radiative cooling. His models suggest that the condensations are part of the shocks. These structures can be expected to contribute to line emission observed in the UV and optical regions.

Since θ^1 Ori C rotates so slowly, it is appropriate to think of this circulation as a rigid, axisymmetric structure comprised of dense blobs. We expect that the circulation we have described is related to the Hα flux and radial-velocity variations (S96; Gagné et al. 2005). An additional consistency check for this infall picture is the *absence* of evidence for a cool, static disk in the magnetic equatorial plane. Such disks are the hallmarks of UV-variable Bp stars. Our modeling of disks for early and late-type Bp stars using *SYNSPEC* and *CIRCUS* (e.g., SG01; Smith 2003) suggests that the disk temperature is typically $0.6\,T_{\text{eff}}$, which for θ^1 Ori C implies a disk temperature near 25,000 K. The ultraviolet line opacity tends to decrease with temperature in this temperature range. Yet even for temperatures as high as 30,000 K, our modeling experiments suggest that a geometrically thin disk with a column density of 10^{22} cm^{-2} in H should be detectable as an absorption feature near rest velocity in the C IV resonance doublet.

The fact that a static disk is *not* visible implies that the circulating component of the wind interior to the Alfven radius must be transported somewhere else. We believe the redshifted emission at ϕ=0.5 is evidence of this transport. Donati et al. (2002) noted that they were unable to duplicate the significantly blueshifted (≈ -75 km s^{-1}) Hα emission in their simulation at the pole-on phase ($\phi = 0.0$). They found that the profile was formed mainly from a static disk, which in their model has a radius of $\sim$3 $R_\star$. It is not surprising that the contribution from such a large disk would dominate the contribution from the polar wind, but the disk cannot produce a blueshifted feature at $\phi = 0$ in this geometry.

Perhaps the blueshifts are caused by the acceleration of jet-like wind from the pole? We have investigated this possibility with *CIRCUS*. We find that even with generous values for relevant parameters the contribution of a jet produces negligible Hα emission relative to the photospheric flux. Moreover, it is even more difficult for a jet-emission model to work for He II λ4686. In contrast, our same modeling experiments demonstrate that for similar temperatures and densities, a much smaller volume viewed beyond the projected face of the star could easily produce the observed Hα emission. From these results we speculate that these blueshifts at $\phi = 0$ have the same cause as the UV resonance line redshifts at $\phi = 0.5$: i.e., they arise from the projection of the component of post-shock matter falling obliquely toward the star, as indicated by the closed arrowheads in Fig. 1.

4.   Summary

From archival *IUE* spectra of the magnetic O-type star θ^1 Ori C, we have discovered new variations of the C IV and N IV resonance doublets, as well as the strong, excited lines of O V λ1371 and N IV λ1718. We found strong similarities between these variations and those exhibited by several prominent optical lines reported in the literature, including Hα and He II λ4686. Lines with the largest variations exhibit an anticorrelation in blue-

and red-wing fluxes at $\phi \approx 0.5$: as the red wing weakens, the blue wing strengthens. In addition to this dichotomy, extractions of the profiles over different velocity bins show that the "M"-shaped wave form present in optical lines is also present in the C IV lines. This morphology disappears at the highest wind velocities sampled (i.e., at the most blueshifted wavelengths), where a single-peaked absorption at $\phi = 0.5$ replaces the "M"-pattern.

The high-velocity strengthenings of the blue wing of C IV at $\phi = 0.5$ are explained by the flow geometry of ud-Doula's MHD simulations. These predict that radiative forces open the field lines and carry them away from the star once they extend beyond the Alfven radius (i.e., several tenths of a stellar radius above the surface; Gagné et al. 2005). At $\phi = 0.5$, the enhanced blue wings of these lines represent material accelerating away from the star along the magnetic plane. We also argued that at $\phi \approx 0.3$ and 0.7 the observer looks along a smaller projected path length through flows that have moderate outward velocities. This means that the excess absorptions at these phases are weaker than the absorptions formed over the longer path length of the open, high-velocity flow viewed at $\phi = 0.5$ (Fig. 1).

The red variations at the edge-on phases ($\phi = 0.5$), which we interpret as emission, require a more complicated geometry in which post-shock material flows towards the star, likely as dense clumps. The presence of this material is also predicted by ud-Doula's simulations, though in the current generation of models the infalling material only occurs episodically.

Finally, *in contrast to bona fide Bp stars, there is no evidence for a cool, static disk.* If post-shock material were to accumulate, given reasonable extrapolations from models of Bp-star disks, a disk ought to be visible in spectra of θ^1 Ori C. We conclude that such accumulation does not happen in the circumstellar environment of θ^1 Ori C.

REFERENCES

Babel, J., & Montmerle, T. 1997, ApJ, 485, L29

Donati, J.-F., Babel, J., Harries, T. J., Howarth, I. D., Petit, P., & Semel, M. 2002, MNRAS, 333, 55

Gagné, M., Caillault, J., Stauffer, J. R., & Linsky, J. L. 1997, ApJ, 478, L87

Gagné, et al. 2005, ApJ, submitted

Groote, D. & Hunger, K. 1976, A&A, 52, 303

Henrichs, H. F., et al. 1998, Ultraviolet Astrophysics beyond the Final IUE Archive, ESO SP-413, 157

Henrichs, H. F. 2005, in ASP Conf. Ser., Workshop on Disks around Stars, ed. R. Ignace, in press

Morgan, W. W., & Keenan, P. C. 1973, ARA&A, 11, 29

Reiners, A., Stahl, O., Wolf, B., Kaufer, A., & Rivinius, T. 2000, A&A, 363, 585 [R00]

Shore, S. N., & Brown, D. N. 1990, ApJ, 365, 665 [SB90]

Shore, S. N., Bohlender, D. A., Bolton, C. T., North, P., & Hill, G. M. 2004, A&A, 421, 203

Short, C. I, & Bolton, C. T. 1994, IAU Symposium 162, Pulsation, Rotation, & Mass Loss in Early-Type Stars, ed. L. A. Balona, H. F. Henrichs, & J. M. LeContel (Dordrecht: Kluwer), p. 171

Smith, M. A. & Groote, D. 2001, A&A, 372, 208 [SG01]

Smith, M. A. 2001, ApJ, 562, 998

Smith, M. A. 2003, in ASP Conf. Ser. 305, Magnetic Fields in O, B, and A Stars, ed. L. A. Balona, H. F. Henrichs, & R. Medupe, (San Francisco: ASP), 310

Stahl, O., et al. 1996, A&A, 312, 539 [S96]

Stahl, O., et al. 1993, A&A, 274, L29

ud-Doula, A., & Owocki, S. P. 2002, ApJ, 576, 413

Walborn, N. R., & Nichols, J. S. 1994, A&A, 425, L29

This manuscript was prepared with the AAS LATEX macros v5.2.

Figure Captions

Figure 1 A sketch (not to scale) of the suggested wind/dipolar magnetic-field orientation
for θ^1 Ori C at $\phi = 0.0$ (from top), 0.3 and 0.7 (from 2 o'clock position), and 0.5
(from right), assuming angles $i = \beta = 45°$. In this planar projection we have collapsed
the observer's positions at $\phi = 0.3$ and 0.7, since they are at equal angles in and
out of page, respectively. The stellar wind expands freely only from the regions
near the magnetic poles (top and bottom of the star). The magnetic field causes
radiatively-driven material from other regions of the stellar surface to follow flux
lines toward the magnetic equator. The wind is divided into two zones according to
its position relative to the star's Alfven radius, which is designated by the dotted
locus and the "X" on the line-of-sight from the center of the star to the observer
(dashed line). Beyond this radius radiative forces dominate over magnetic forces
and cause the wind to accelerate away from the star, approximately parallel to the
magnetic equatorial plane. Within the Alfven radius, wind particles emerge from
near the magnetic poles, follow closed loop lines (open arrowheads), and encounter
streams from the opposite hemisphere at the magnetic equator, where they shock
and accumulate. Periodically, the particles formerly in the wind condense into
optically thick blobs, which return to the star along the original field lines (full
arrowheads). The redshifted variations suggest that the post-shock gas falls at speeds
of $300 - 400$ km s^{-1}.

Figure 2: Dynamic spectrum of the 22 high-dispersion *IUE* echellograms of θ^1 Ori C
obtained through the large-aperture with the SWP camera showing variations in the
C IV $\lambda\lambda$1548, 1551 doublet as a function of magnetic/rotational phase. The shading
represents differences with respect to the time-averaged mean spectrum (lower panel):
darker shades denote phases and wavelengths where the profile is deeper (i.e., less

flux) than its time-averaged value. The difference spectra have been smoothed over ~1 Å. Phase gaps in this spectrum are due to the paucity of observations. Brackets in the lower panel indicate the extent of the blue and red components of the doublet for an assumed terminal velocity of 2500 km s^{-1} (S96). Although the dominant variations occur in the blue wing of the absorption trough (window "a"), significant variations occur throughout the profile. The variations in window "e" are anti-correlated with those in window "a."

Figure 3: Three high-resolution *IUE* spectra in the region of the C IV resonance lines for phases $\phi = 0.51$, 0.60, and 0.94 (SWP 54040, SWP 07481, and SWP 14665). The units for the flux are erg s^{-1} cm^{-2} Å^{-1}. All spectra are binned over 4 pixels, which undersamples the line cores and give them a sharp appearance. The spectra obtained at $\phi = 0.60$ and 0.94 (solid and dashed lines, respectively) exhibit the maximum difference in blue- and red-wing flux. Wavelength windows *a–e* are referenced in Figs. 2 and 6. Following S96, phase zero is defined by the epoch HJD=2448833.0 (MJD=48832.5).

Figure 4: *IUE* spectra for phases 0.60 and 0.64 (SWP 07481 and 54058; solid line is their mean) and 0.90 and 0.94 (SWP 54094 and 14665; dashed line is their mean) are compared in the region of the N V doublet of θ^1 Ori C. The spectra have been binned over 4 points. The computed difference spectrum, binned over 8 points, is shown at the bottom in units of erg s^{-1} cm^{-2} Å^{-1}.

Figure 5: Relative equivalent width index (normalized to the maximum value) versus phase for the red members of the C IV and and N V doublets, as extracted over the velocity range between 0 and +250 km s^{-1} (0 – 1.3Å). The dotted line is a reference sinusoid.

Figure 6: Equivalent width index versus phase extracted from four velocity ranges in the

blue wing of C IV λ1548; see windows *"a – e"* in Fig. 2. The curves have been offset vertically for clarity. The corresponding extraction from 1548 Å was not used due to interference with the wind absorption of the 1550 Å line. Note the progression from no variation, to an "M"-like pattern, and finally to a morphology featuring a single peak at $\phi \approx 0.5$.

Figure 7: Equivalent width index variations with phase of the excited O V λ1371 line, as extracted from negative and positive velocities of the line profile.

Fig. 1.— cartoon

Fig. 2.— grysc

Fig. 3.— c4mnmx

Fig. 4.— n5mnmx

Fig. 5.— c4n5phas

Fig. 6.— c4wng

Fig. 7.— o5phas

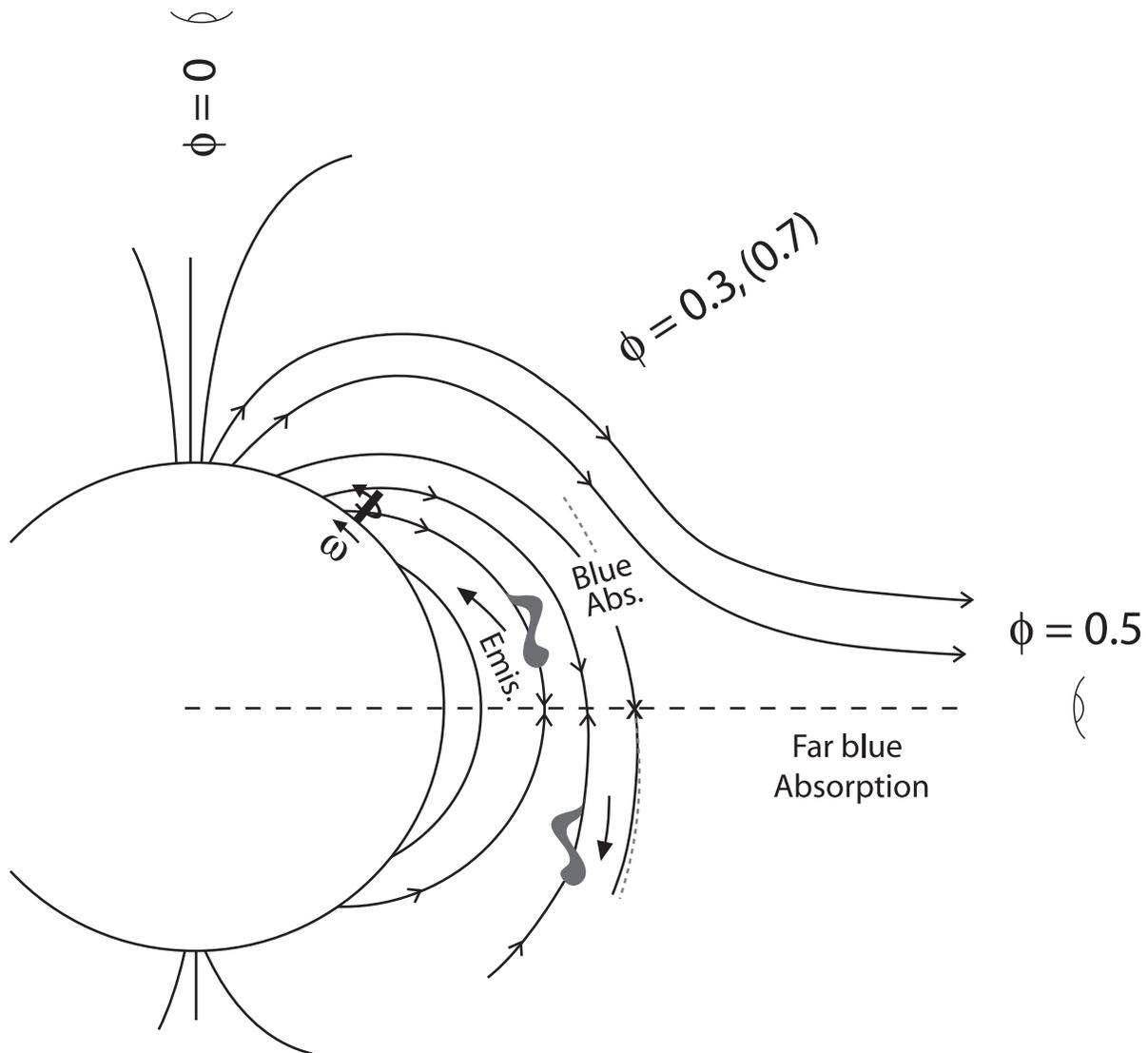Table 1.   Dependence of line strength modulations on rotational phase

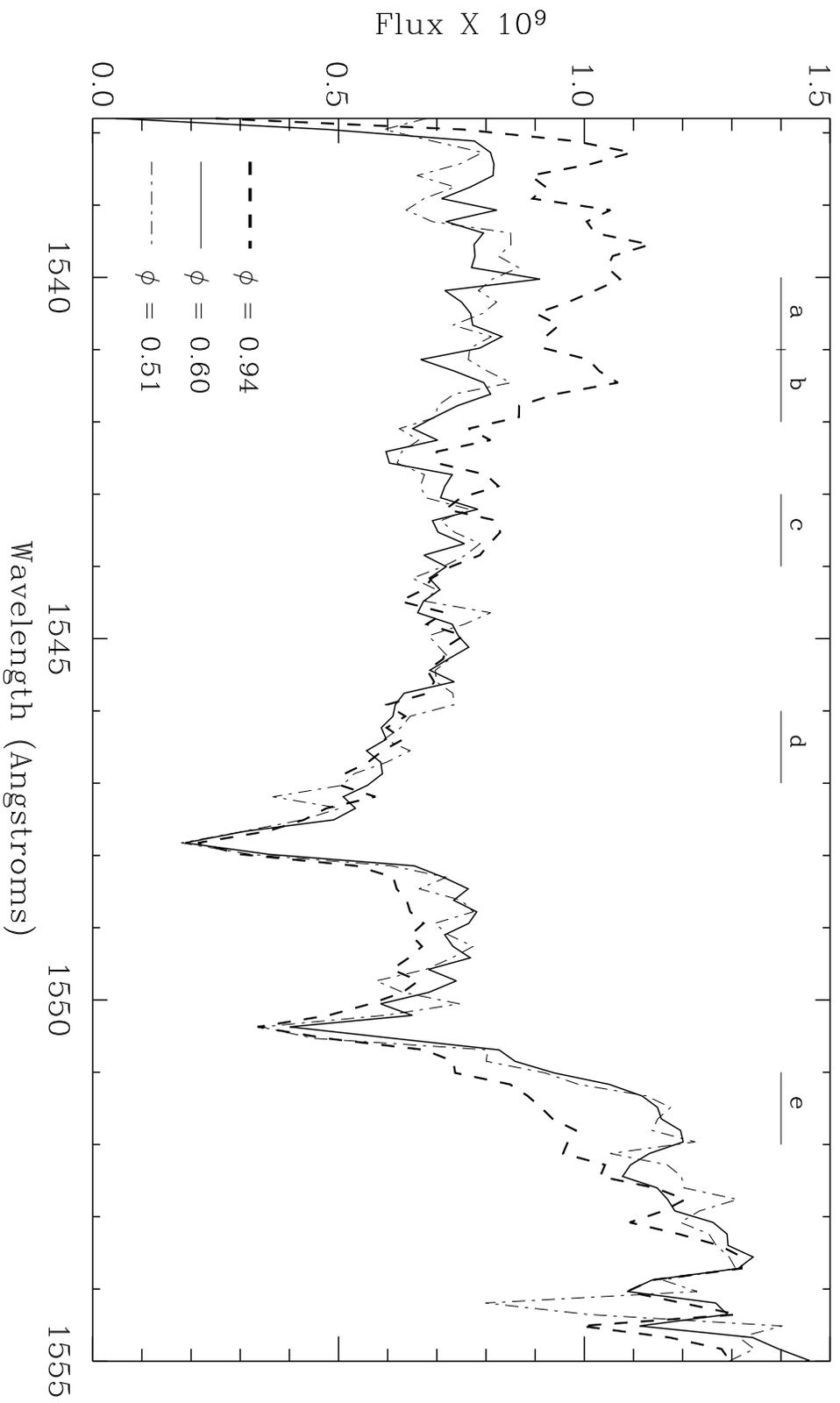| Ion	λ (Å)	χ_{exc}[a]	I.P.[b]	ϕ(Max. EW)	Source[c]
H I	6563	10.2	13.2	$0.4-0.6$	S96-4
He II	4686	48.4	54.4	$0.4-0.6$	S96-5
He I	4471	21.0	24.6	0.0	S96-13
He II	4541	51.0	54.4	0.0	S96-14
C IV	5801	37.5	64.5	0.0	S96-15
C IV	5812	37.5	64.5	0.0	R00-7
C IV	1548, 1550	0.0	64.5	$0.4-0.6$	S96-8
C IV	1548, 1550[d]	0.0	64.5	0.0	Fig. 5
N IV	1718[d]	16.2	77.4	0.0	§ 3.3.3
N V	1238, 1242[d]	0.0	97.9	0.0	Fig. 5
O III	5592	33.9	55.0	0.0	S96-16
O V	1371[d]	19.7	113.9	0.0	Fig. 7
Si IV	1394, 1402	0.0	45.1	$0.4-0.6$	S96-9

[a]Excitation potential for the transition in eV.

[b]Ionization potential for the species in eV.

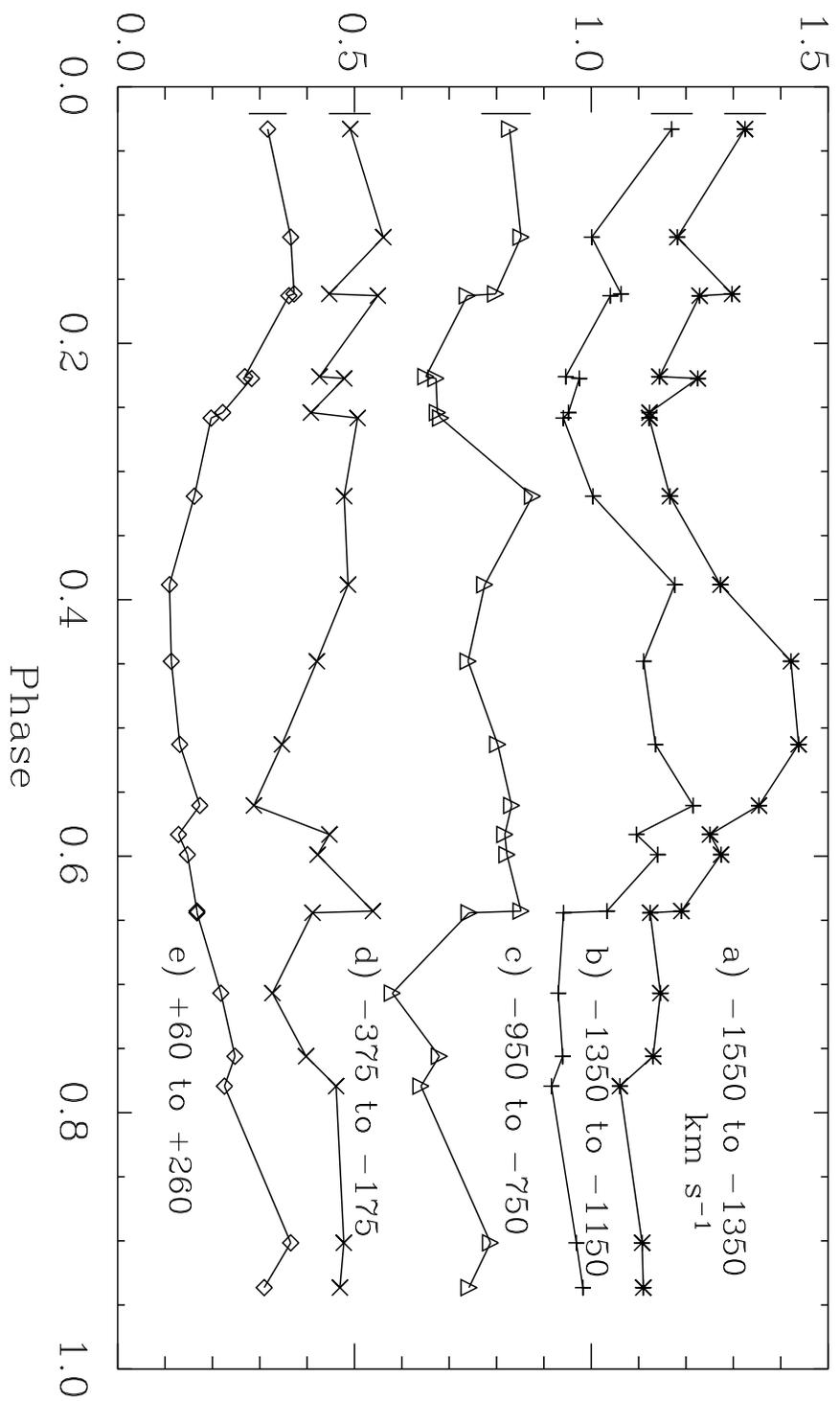[c]The format "Ref-n" refers to figure "n" in reference "Ref."

[d]Red half only.

$\phi = 0$

$\phi = 0.3, (0.7)$

$\phi = 0.5$

ϖ

Blue
Abs.

Emis.

Far blue
Absorption

Relative Equivalent Width

Flux X 10^9

0.0 0.2 0.4 0.6 0.8 1.0

2.0 1.5 1.0 0.5 0.0

1.0 0.8 0.6 0.4 0.2 0.0

$\phi = 0.94$

$\phi = 0.8$

(Edge)

C IV

N V

N V

(Reseaux)

N V

C III

N V

1236 1238 1240 1242 1244 1246 1248

Wavelength (Angstrom)

0.0 0.2 0.4 0.6 0.8 1.0

Phase

EW Indices for θ Ori[1] C

Phase

a) -1550 to -1350 km s^{-1}

b) -1350 to -1150

c) -950 to -750

d) -375 to -175

e) $+60$ to $+260$

EW Indices for 1371A

◇ 1370-1371 A
✳ 1371-1372 A (shifted by -.7)

Phase